Chemical Engineering Journal 470 (2023) 144053

Contents lists available at ScienceDirect

Chemical Engineering Journal

journal homepage: www.elsevier.com/locate/cej

Electron transfer process in dechlorination of polychlorinated biphenyls (PCBs) by nickel/zero-valent iron: Effects of temperature and selectivity pattern

Yingxin Wu [a,b], Jingyan Zhou [a], Zhuohao Wu [a], Quanyun Ye [a,b,*], Wencheng Wu [a,b,*], Xiaowen Liu [a], Dechun He [a,b], Guifang Lv [a], Jie Zhang [a]

[a] South China Institute of Environmental Sciences, Ministry of Ecology and Environment, Guangzhou 510655, China
[b] Guangdong Engineering & Technology Research Center for System Control of Livestock and Poultry Breeding Pollution, Guangzhou 510655, China

ARTICLE INFO

Keywords:
Polychlorinated biphenyls
Zero-valent iron
Dechlorination pathways
Quantum chemistry calculation

ABSTRACT

The dechlorination of polychlorinated biphenyl (PCB) has been studied intensively, while the comprehensive understanding of the electron transfer and selectivity pattern mechanism is still limited. Therefore, in this study, the reactivity of nickel/zero-valent iron (Ni/Fe) was investigated during the dechlorination of 2,2′,4,4′,5-pentachlorobiphenyl (PCB-99) at various temperatures. Gas chromatography-mass spectrometry analysis and quantum chemical calculations, including bond dissociation energy, C-Cl bond length, and the lowest unoccupied molecular orbital (LUMO), were used to explore the dechlorination pathways and the electron selectivity. Results showed that the reduction efficiency of PCB-99 (100 μg L^{-1}) did not increase monotonically with the temperature, but followed the order: 25 °C (75.9%) > 15 °C (62.5%) > 35 °C (51.6%), due to the thermodynamic evolution of Fe species to generate more Fe(II) and the abundance of oxygen vacancies at 25 °C. However, as the temperature continued raising to 35 °C, Ni/Fe was oxidized heavily and aggregated into large particles, significantly reducing the electron density of Fe(II) and inhibiting the electron transfer. The main dechlorination pathway was PCB-99 → PCB-47 → PCB-17 → PCB-8 → PCB-3 → biphenyl, indicating that electrons tended to attack C-Cl bonds following the order *meta-* > *para-* > *ortho*-position, which could be better explained by LUMO. Overall, this work is expected to improve the understanding of the dechlorination behavior of PCB-99 from both fundamental and applied perspectives.

1. Introduction

Zero-valent iron (ZVI, Fe^0) has attracted extensive attention for the reduction of chlorinated organic compounds (COCs) in various environmental media due to its low price, strong reducibility, and the environmental benign of iron[1–3]. The core–shell structure of the Fe^0 core and the iron oxide layer leads to the unique ZVI surface for adsorbing and transforming pollutants[2]. As a heterogeneous catalysis, the interfacial reaction mediated by ZVI can be strongly influenced by the surficial properties. Typically, unmodified ZVI particles tend to agglomerate into large particles and generate an oxide layer on the surface, resulting in inferior reaction activity and low stability, as the electron transfer process is hindered[4,5]. Therefore, to overcome the abovementioned shortcomings, ZVI is usually modified with metal catalyst (such as Cu[6], Ni[7], and Pd[8], etc.) to form bimetals, which could accelerate the electron transfer effectively.

Extensive studies have been conducted to understand the effect of reacting conditions on the reactivity of ZVI and bimetals, which is closely related to the electron transfer process. These parameters include pH, applied dosage and temperature. To the best of our knowledge, the research conclusions about pH and dosage are basically consistent. For example, larger dosage of ZVI (or bimetals) and lower pH usually lead to more efficient reduction as more electrons are generated under these conditions[9,10]. However, effects of temperature on the dechlorination by ZVI or bimetals remain controversial. Several researchers have proved that the kinetic rate constants increased with increasing temperature during the dechlorination, which is generally caused by the facilitation of electron transfer. To be specific, electron transfer to the target compounds from ZVI (or bimetals) surface is promoted due to the lower activation energy (E_a) for dechlorination and the increase in the

* Corresponding authors at: South China Institute of Environmental Sciences, Ministry of Ecology and Environment, Guangzhou 510655, China.
E-mail addresses: quanyunye@scies.org (Q. Ye), wuwencheng@scies.org (W. Wu).

https://doi.org/10.1016/j.cej.2023.144053
Received 11 April 2023; Received in revised form 7 June 2023; Accepted 9 June 2023
Available online 10 June 2023
1385-8947/© 2023 Elsevier B.V. All rights reserved.

energy levels of the involved reactants[11,12]. In contrast, other researchers argued that temperature had little effect on the dechlorination [13]. Moreover, high temperature will lead to the rapid formation of passivation layer and then significantly inhibit the electron transfer[14]. Consequently, a systematic study on ZVI reactivity, especially on the electron transfer process at different temperatures is urgently needed from both fundamental and applied points of view. Further, the transferred electrons do not react indiscriminately with the target compounds. Normally, electrons react with the C-Cl bonds following a stepwise dechlorination process with certain selecting patterns of positions. However, there is limited knowledge regarding the mechanisms of this selectivity, which greatly hinders the needed process for reasonably assessing and controlling the potential environmental risks. Therefore, an accurate quantum descriptor is desperately needed for explaining the selectivity and predicting the dechlorination pathways.

To understand the electron transfer process during the dechlorination mediated by ZVI (and bimetals), the hydrophobic and recalcitrant polychlorinated biphenyls (PCBs)[15–17] are selected as the model target compounds in this study. They are a group of persistent organic pollutants that, up until the early 1970 s, were widely used in a variety of commercial and chemical industries[18,19] and had negative effects on both the environment and human health[20]. Despite the ban or restriction of PCBs in most countries, there still left an environmental legacy[21–24]. To make it worse, illegal dismantling of e-waste and incineration of PCB-containing waste contribute continuously to the release of large quantities of PCBs into the environment[25,26]. Once released, PCBs can spread in almost all environmental media, raising an urgent need for efficient dechlorination, such as biological[27–29] and chemical methods[30]. To be specific, 2,2′,4,4′,5-pentachlorobiphenyl (PCB-99) was selected as the target pollutant because it possesses chlorine substituents at *ortho*-, *meta*-, and *para*- positions on benzenes, making it possible to identify the selectivity of electrons at different positions. A total of 24 dechlorinated congeners can be derived from PCB-99, of which the physicochemical characteristics may vary greatly. Their molecular orbital information was obtained by three common quantum chemistry methods, including bond dissociation energy, C-Cl bond length, and the lowest unoccupied molecular orbital (LUMO), which could measure the difficulty for cleavage of chemical bonds and characterize the electron acceptance characteristics of the compound. Moreover, the dechlorinated products were determined by gas chromatography-mass spectrometry (GC–MS) to confirm the selecting patterns of electron.

Overall, this study aims to elucidate the electron transfer process in the dechlorination mediated by Ni/Fe as a representative of bimetals. The objectives of this study are (i) to investigate the influence of temperature on Ni/Fe reduction efficiency and the mechanism; (ii) to propose the electron selecting pattern by identifying the dechlorination products and pathways of PCB-99 based on GC–MS analysis and quantum chemistry calculation. The findings are expected to improve the understanding of the electron transfer process during the dechlorination mediated by Ni/Fe.

2. Materials and methods

2.1. Materials

Carbonyl iron was obtained from D-BASF Company, Germany. Standard solution of PCB-99 (≥99.6%), 2,2′,3,3′,4-pentachlorobiphenyl (PCB-82, ≥ 99.7%), 2,3,5,6-tetrachlorobiphenyl (PCB-65, ≥ 99.7%), and other mentioned PCB congeners in this study were purchased from Dr. Ehrenstorfer, Germany. Nickel sulfate hexahydrate ($NiSO_4{\cdot}6H_2O$, ≥ 99.9%), ethanol (CH_3CH_2OH), normal hexane (*n*-hexane, C_6H_{14}), acetone (CH_3COCH_3), aluminum oxide (Al_2O_3), silica gel (SiO_2), and anhydrous sodium sulfate (Na_2SO_4) were purchased from Shanghai Aladdin Biochemical Technology Co., LTD, China. All the chemicals and reagents were used without further purification.

2.2. Synthesis and characterization of Ni/Fe

The synthesis of Ni/Fe was shown in Text S1, Supporting Information (SI). Details of Ni/Fe characterizations before and after reactions, such as X-ray diffraction (XRD), X-ray photoelectron spectroscopy (XPS), field emission scanning electron microscopy (FESEM) with energy-dispersive X-ray (EDX) were described in Text S2, SI.

2.3. Dechlorination experiments

In the anaerobic chamber, batch experiments for PCB-99 dechlorination were carried out in a Teflon bottle with 100 mg of freshly prepared Ni/Fe samples and 50 mL of PCB-99 solution (100 μg L^{-1}), based on the results of our previous optimization experiments[31]. Dechlorination experiments were conducted in shaking incubator with a constant temperature of 15, 25, or 35 ℃, and a rotation speed of 15 rpm. The temperature setting range was similar to the temperature range of actual PCBs contamination remediation, which was more significant for research. All experiments in this study were carried out in triplicate. As PCBs are hydrophobic, to extract all of them from both solid and liquid phases at scheduled time intervals, totally 15 mL of *n*-hexane was added to each vial in 3 batches and mixed thoroughly before collection. PCB-99 on both solution and the surface of Ni/Fe could be extracted to avoid the interference of adsorption on dechlorination results. The collected *n*-hexane solutions were then combined and concentrated to 1 mL before purification by neutral aluminum oxide and neutral silica gel, and dehydrated by anhydrous sodium sulfate. Afterward, the solution was concentrated to 500 μL before determination[32]. Detailed parameters of determination were described in Text S2, SI. The method detect limit of PCB-99 was 1 ppb.

Quality assurance and quality control was achieved by adding PCB-65 as surrogate to each sample before extraction. The quantification of PCB-99 was calculated using PCB-82 as an internal standard. The recovery of PCB-65 ranged 72.3–83.0%, while the recovery rate of PCB-99 in the blank controls (treatments containing PCB-99 and deoxidized deionized water but without Ni/Fe) was 84.9–94.1%.

2.4. Quantum chemistry calculation

All calculations of PCB-99 and dechlorinated congeners were performed by the Gaussian 16 quantum chemistry software[33]. At the level of B3LYP/6-311G+(d, p), the structure of each PCB monomer was optimized in the ground and excited states. On the basis of structure optimization, frequency calculation and analysis were carried out to ensure that each structure did not contain virtual frequency. GaussView 6 software was used to image the molecular orbitals of PCB congeners in the ground and excited states. The molecular structures were optimized to obtain the LUMO configuration, and the relationship between the molecular structure, LUMO configuration, and energy was analyzed [34,35].

The reaction of C-Cl bond breaking is as follows:

$$PCB = PCB\bullet + Cl\bullet \quad (1)$$

The bond dissociation energy (ΔE_r) of C-Cl bonds can be calculated using the following formula:

$$\Delta E_r = E_{PCB\bullet} + E_{Cl\bullet} - E_{PCB} \quad (2)$$

where $E_{PCB\bullet}$ is the single point energy of PCB• for removing a Cl• free radical, $E_{Cl\bullet}$ is the single point energy of Cl• free radical, and E_{PCB} is the single point energy of PCB. The calculation process includes the correction of zero-point energy.

3. Results and discussion

3.1. Characterization of Ni/Fe

The morphology of as-synthesized samples was analyzed using SEM (Fig. 1(a) and (b)) coupled with EDX to confirm the composition of Ni/Fe (Fig. 1(c)). ZVI particles were generally spherical in shape with diameter sizes ranging from 0.5 to 4 μm, while no obvious difference in both particle size and shape was observed after Ni loading. Spherical particles tended to stick together due to the interaction of geomagnetic forces and surface tension between small particles[36]. The EDX result revealed that the compositional distribution of three elements (Fe, Ni, and O) in Ni/Fe, among which the loading of Ni was approximately 0.5%, further proving the successful synthesis of Ni/Fe. Compared with ZVI particles, Ni/Fe could form electric couples, which would lead to an increase in electron transfer through the difference in corrosion potential between Fe and Ni, thus improving the dehalogenation efficiency [37,38].

The crystal structures of ZVI and Ni/Fe were determined by wide-angle XRD (10°~80°), as shown in Fig. S1. ZVI exhibited characteristic diffraction peaks at $2\theta = 44.68°$ and 65.30°, corresponding to the (1 1 0) and (2 0 0) lattice facets of Fe^0, respectively (JCPDS 06–0696). Ni/Fe also exhibited similar diffraction peaks at $2\theta = 44.68°$ and 65.06°, which corresponded to the (1 1 0) and (2 0 0) lattice planes of iron nickel, respectively (JCPDS 65–7251). It was demonstrated that the characteristic peaks of Fe and Ni were close to each other and difficult to distinguish[39,40]. A broad amorphous peak could be seen at 2θ ranging from 20° to 30°, which was the amorphous peak of the hydroxides of iron. Additionally, the average particle size of ZVI and Ni/Fe could be calculated by Scherrer equation (Text S3, SI) as 6.88 nm and 6.55 nm (Table S1 and S2), respectively, indicating that the particle size of ZVI was hardly affected by Ni loading.

XPS was employed to analyze the oxidation state of the freshly prepared Ni/Fe. The wide-scan survey was shown in Fig. 2(a), and the high-resolution spectra of Ni 2p, Fe 2p, and O 1 s were presented in Fig. 2 (b), (c) and (d), respectively. It could be seen that Ni/Fe was mainly composed of iron, nickel, and oxygen, which was consistent with the previous EDX results. For Ni 2p, the peaks at 856.3 eV in Ni 2p3/2 orbit and 873.7 eV in Ni 2p1/2 orbit correspond to Ni^0, while the peaks at 862.2 eV and 879.6 eV were the satellite peaks[39,41], indicating that the Ni on the surface of Ni/Fe was mainly in the form of Ni^0. For Fe 2p, two main peaks at approximately 710.7 eV (Fe 2p3/2) and 724.5 eV (Fe 2p1/2), and a shoulder peak at 718.3 eV (shake-up satellite of Fe 2p3/2) could be observed[42]. The peaks at ~ 713.0 eV and ~ 725.7 eV were ascribed to Fe(III), while the peaks at ~ 710.3 eV and ~ 723.6 eV were assigned to Fe(II)[43]. Fe(II) was formed due to either oxidation of the underlying Fe^0 and/or (Fe^0-mediated) reduction of the Fe(III) passivating layer[44]. Consistent with previous reports[45], the peak at approximately 706.1 eV corresponding to Fe^0 2p3/2 was barely observable because Ni/Fe was coated with iron oxide shell and Fe^0 existed below the surface. The thickness of this shell would likely increase with the progress of the Fe^0 oxidation. The O 1 s spectrum showed three contributions, the peak at ~ 529.1 eV (O1) was assigned to the lattice oxygen (O^{2-}), the peak at ~ 530.7 eV (O2) could be ascribed to surface-adsorbed oxygen species (O_2^-,O_2^{2-}, or O^-), while the peak at ~ 532.3 eV (O3) was caused by the surface-adsorbed water[46]. It was reported that the content of the surface-adsorbed oxygen species was related to surface oxygen vacancies[47], which would greatly affect the redox activity of Ni/Fe.

3.2. Effects of temperature on PCB-99 dechlorination

Effects of temperature on PCB-99 dechlorination were studied at 15–35 °C, which were similar to those in the actual remediation process. The kinetic curves of PCB-99 dechlorination by Ni/Fe at different temperatures were shown in Fig. 3. At 15 °C and 25 °C, the content of PCB-99 decreased rapidly in the first 2 h of reaction. However, the reaction slowed down afterward and gradually reached equilibrium after 48 h.

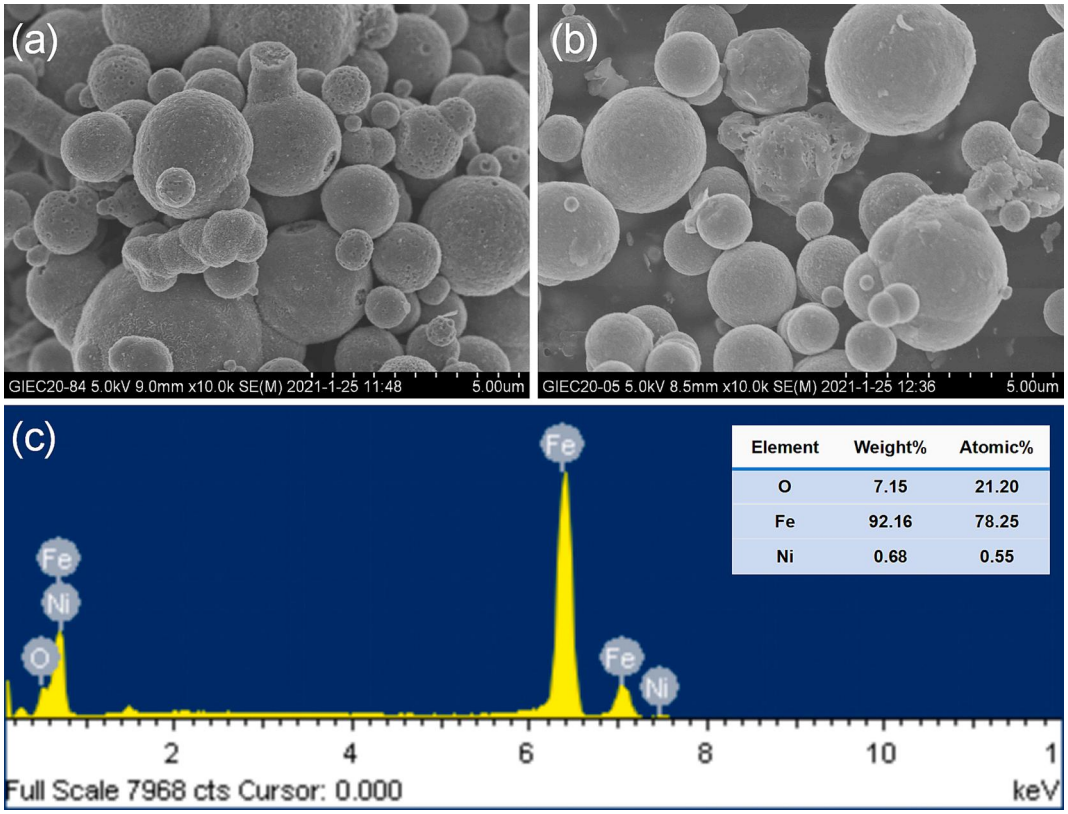

Fig. 1. The SEM photographs of (a) ZVI: magnification of 10 K×; (b) Ni/Fe: magnification of 10 K×; (c) The EDX image of Fe, Ni, and O in Ni/Fe.

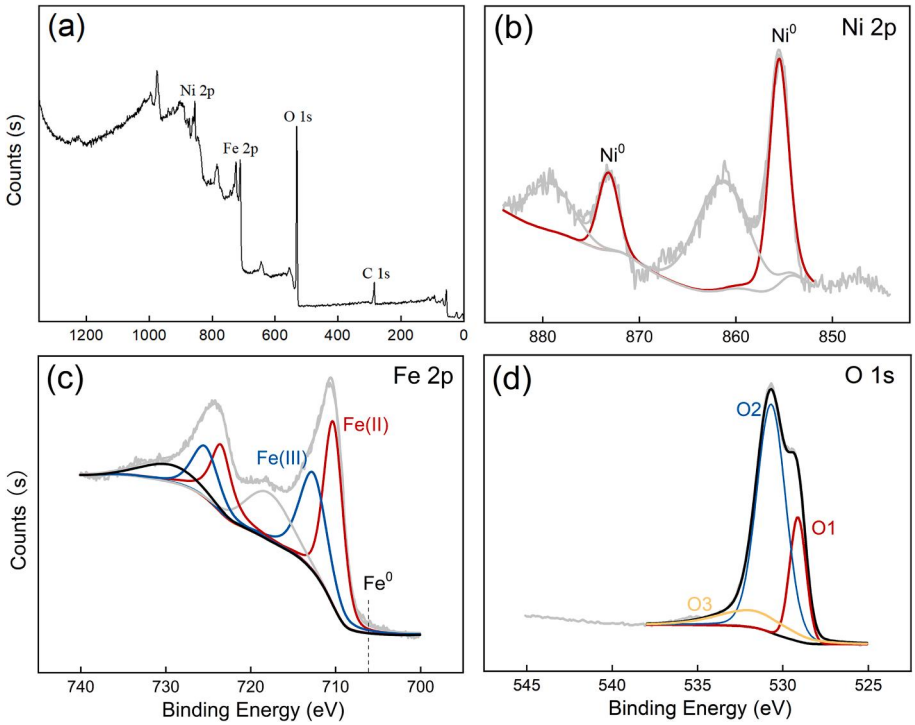

Fig. 2. (a) XPS wide-scan survey of Ni/Fe; (b) Ni 2p high-resolution spectrum; (c) Fe 2p high-resolution spectrum; (d) O 1 s high-resolution spectrum.

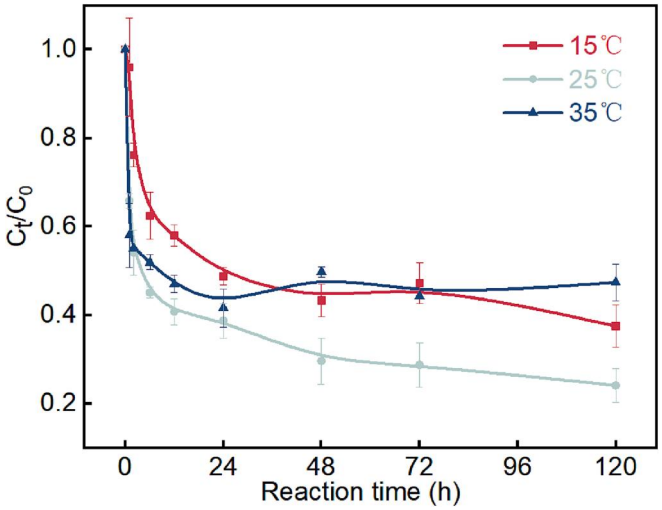

Fig. 3. Kinetic curves of the PCB-99 dechlorination by Ni/Fe at different temperatures. Reaction conditions: 50 mL of PCB-99 solution (100 μg L^{-1}), 100 mg of Ni/Fe and initial pH unadjusted.

This could be attributed to the oxidation of Fe^0 and the formation of oxide coating on the surface of Ni/Fe[45]. Within 120 h, the dechlorination efficiency of PCB-99 at 25 °C could reach 75.9%, which was much higher than that (62.5%) at 15 °C ($p = 0.0006$). This might be attributed to the enhanced electron transfer by temperature, as the process was thermodynamic. However, the reactivity of Ni/Fe did not increase monotonically, but decreased with further increase of temperature. At 35 °C, the dechlorination process was accelerated. The content of PCB-99 decreased rapidly in the first 1 h, then the reaction slowed down and reached equilibrium after 24 h. The dechlorination efficiency of PCB-99 within 120 h was only 51.6%. This finding was somewhat unexpected regarding the previous studies of ZVI applications that high temperature increased the efficiency of reduction[48]. Since high temperature promoted both the electron transport to PCBs and the Fe oxidation simultaneously, this unusual trend could not be simply demonstrated by the molecular motion theory. One possible explanation for the reduced reactivity of Ni/Fe at 35 °C might be the rapidly forming oxide layer significantly inhibited the electron transfer from the Fe^0 core to the outermost surface.

3.3. *Mechanism underlying the influence of temperature on PCB-99 dechlorination by Ni/Fe*

As known, heterogeneous dechlorination mediated by ZVI and bimetals depended on both mass transfer and electron transfer processes. Previously, we confirmed that almost 100% of the hydrophobic PCB-99 distributed on the Ni/Fe particles in this system throughout the entire course[49]. Therefore, the oxide layer did not significantly influence the mass transfer process. The influence on reactivity therefore was mainly ascribed to the electron transfer process. In order to better explain the influence mechanism of temperature, the morphology changes, degree of oxidation, and iron oxide species of Ni/Fe were analyzed.

3.3.1. *Effects of temperature on the morphology and structure of Ni/Fe*

Stability is critical for Ni/Fe because the enhanced reactivity is imparted by its large specific surface area. However, bimetallic materials inevitably reacted with water and oxygen during the reaction[50], and the reactivity of the bimetallic materials could be affected by surface morphology, particle size, and particularly the degree of oxidation, most likely as a result of the ability for electrons to diffuse more easily to the surface of the bimetallic materials and the larger available reactive surface area[51]. To understand the effects of temperature on the reaction, the morphology and structure of Ni/Fe were characterized. It could be seen from Fig. 4(a) that the surface of fresh Ni/Fe was smooth, which became rough after 48 h of reaction (Fig. 4(b)-(d)), indicating the oxidation of Ni/Fe. As expected from the above-mentioned results, the surface of Ni/Fe was the coarsest after the reaction at 35 °C, it was explained that the reaction of Ni/Fe with water or oxygen was greatly accelerated at 35 °C due to the enhancing thermal motion of molecules and the galvanic effect between Fe and Ni[37]. Certain amount of Ni/Fe

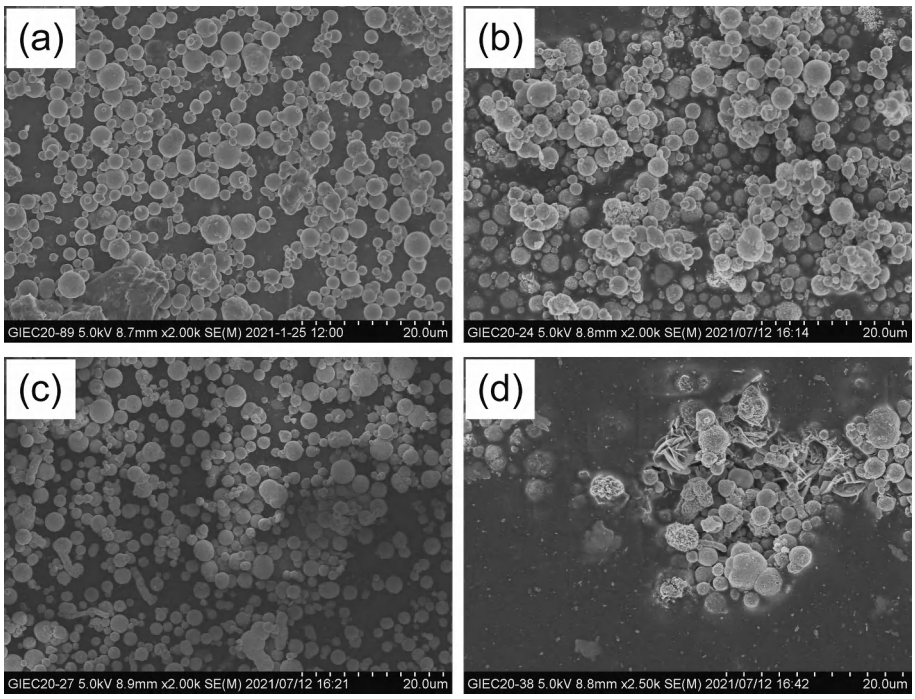

Fig. 4. SEM images of Ni/Fe before reaction (a) and after reaction at 15 °C (b), 25 °C (c) and 35 °C (d) for 48 h.

aggregated to form many larger particles and even converted into layered iron oxide, which significantly reduced the active sites for PCB-99 dechlorination and was detrimental to the ability of particles to remain suspended for a prolonged period[52]. Similarly, the reductive reactivity of Ni/Fe was also influenced by its aggregation state, with the larger aggregates imparting the lower reactivity. The results indicated that increasing the temperature from 25 °C to 35 °C could only increase the electron production of Ni/Fe, rather than effectively improve the electron selectivity. Temperature rise would cause more electrons to react with oxygen or other oxidizing substances, resulting in greater oxidation degree of Ni/Fe surface, which in turn would hinder the reaction with target compounds.

3.3.2. *Effects of temperature on the iron oxide species of Ni/Fe*

As previously reported[53,54], the reduction efficiency could be significantly influenced by the iron oxide species on ZVI surface, as they provided distinct site density, surface speciation, and Fe(II) contents. Therefore, the high-resolution spectra of Fe 2p and O 1 s at different

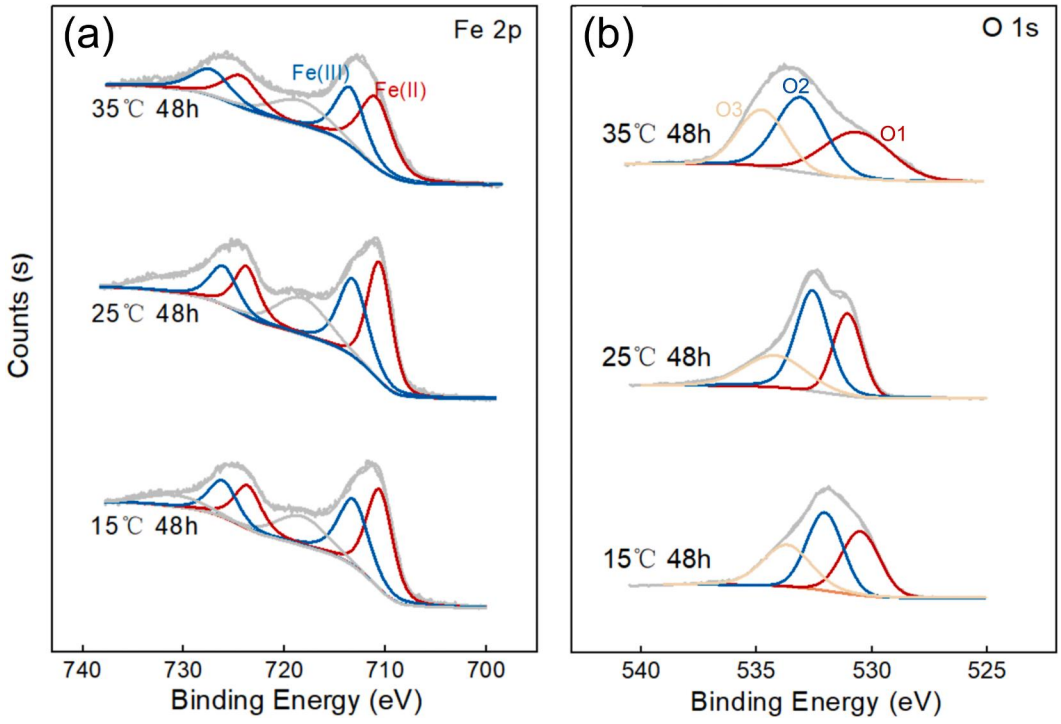

Fig. 5. (a) Fe 2p and (b) O 1 s spectra of Ni/Fe after 48 h reaction at different temperatures.

temperatures after 48 h of reaction were analyzed. Fig. 5(a) revealed that the peak intensity of Fe(II) decreased compared with that of fresh Ni/Fe (Fig. 2(c)) after 48 h, indicating the decrease of the Fe(II) content. Moreover, the peak intensity of Fe(II) at different temperature was in the order of 25 °C > 15 °C > 35 °C. Surface-bound Fe(II) on the oxide surface could play an important role in enhancing PCB-99 reduction by Ni/Fe due to the increase in electron density of Fe(II)[54,55]. Therefore, the larger amount of Fe(II) on Ni/Fe surface was one of the reasons for the better reactivity at 25 °C. This is consistent with an aging study under strictly anoxic conditions at both distinct temperatures. It was reported that nearly 70% of the Fe^0 was transformed to $Fe(OH)_2$ after 3000 h at 25 °C, while it only took 200 h to transform to Fe_3O_4 at 80 °C[56]. The thermodynamic Fe evolution process could be accelerated by higher temperature. However, as the process continued, Fe(II) would be further oxidated and converted to Fe(III), which passivated the Ni/Fe surface, leading to the inhibition of electron transfer from the Fe^0 core to the outermost surface[57,58]. More importantly, a decrease in the amount of surface Fe(II) would reduce the electron density[54], thus causing the decrease of PCB-99 dechlorination efficiency, as in the case of 35 °C.

Likewise, Fig. 5(b) showed that the peak intensity of surface-adsorbed oxygen species (O2) decreased after 48 h compared with that of the fresh Ni/Fe (Fig. 2(d)), proving that the content of surface oxygen vacancies decreased after the reaction. As expected, the surface oxygen vacancies were still the most abundant at 25 °C. The oxygen vacancies provided the most extra catalytic sites and accelerated the electron transfer[59], as they could alter the electric state of iron on the surface of iron oxide and lead to enhanced conductivity[60]. To be specific, these vacancies were able to localize electrons and benefited the reduction reaction[47]. Moreover, the peak intensity of O3 was in the order of 35 °C > 15 °C > 25 °C, which might also positively correlate with the oxidation degree of the Ni/Fe surface, further confirming that temperature at 35 °C increased the electron production rather than improve the electron selectivity. More electrons competitively reacted with oxygen or other oxidizing substances (instead of PCB-99) on Ni/Fe at 35 °C, resulting in greater oxidation degree of Ni/Fe surface, which in turn inhibited the electron transfer and hindered the reaction with PCB-99.

In summary, the better reactivity of Ni/Fe under the reaction condition of 25 °C could be attributed to the enhanced electron transfer due to the thermodynamic evolution of Fe(II) and the abundance of oxygen vacancies. Also, the efficiency of electron transfer varied with the properties of the Ni/Fe surface, which would significantly change during the dechlorination process. Temperature was a parameter to accelerate or postpone the course, rather than alter the route of electron transfer. The lower temperature (15 °C) extended the longevity of Ni/Fe by slowing down the surface oxidation, but was not conducive to dechlorination efficiency (Fig. 3). However, at 35 °C, the surface of Ni/Fe would be heavily oxidized within a short period and the particles aggregation occurred, which reduced the electron density and transfer because of the decrease in the amount of surface Fe(II), thus hindering the further reaction.

3.4. Quantum chemistry calculation

The stepwise dechlorination mediated by ZVI or bimetals would facilitate the understanding of the dechlorination pathway. Previous studies have identified the preferential dechlorination routes (namely the selectivity of electron), while the mechanism remained unclear. The quantum chemistry calculation was able to provide an insight. This method was considered as an important supplement to predict the reaction mechanism of organic pollutants, and the theoretical results were well verified by experimental studies[61,62]. In this study, 5 congeners of tetrachlorobenzene (PCB-74, PCB-66, PCB-49, PCB-48, and PCB-47), 8 congeners of trichlorodiphenyl (PCB-37, PCB-33, PCB-31, PCB-29, PCB-28, PCB-25, PCB-18, and PCB-17), 8 congeners of dichlorinated biphenyls (PCB-15, PCB-13, PCB-12, PCB-9, PCB-8, PCB-7, PCB-6, and PCB-4), 3 congeners of monochlorinated biphenyls (PCB-3, PCB-2, and PCB-1) and biphenyl might be produced during the dechlorination of PCB-99, as shown in Table S3.

3.4.1. Calculation of dissociation energy of C-Cl bond

The C-Cl bond dissociation energies of PCB-99 and the other 24 dechlorinated products were shown in Table S4, which measured the difficulty for cleavage of chemical bonds[63]. Among them, the dissociation energy of *ortho*-position C-Cl on PCBs with only one adjacent substituent was the lowest because the *ortho*-position C-Cl bond would increase the dihedral angle of PCBs and reduce the conjugation of the two benzene rings, indicating that the *ortho*-position C-Cl bond was the most prone to fracture[64]. But no obvious regularity was found in asymmetric PCBs with two *ortho* substituents (PCB-99, PCB-49, PCB-48, PCB-18, and PCB-17). For example, the dissociation energy of *ortho* C-Cl on the benzene ring of PCB-48 with more chlorine substituents (87.2101 kcal mol^{-1}) was lower than that with less chlorine substituents (87.9229 kcal mol^{-1}); however, the dissociation energy of C-Cl bond on the benzene ring of PCB-99 with more chlorine substituents (87.1436 kcal mol^{-1}) was greater than that with less chlorine substituents (86.9817 kcal mol^{-1}). For PCBs with chlorine substituents in *meta*- and *para*-position (such as, PCB-37, PCB-13, and PCB-12), the dissociation energy of *meta*-position C-Cl was lower, demonstrating that the fracture occurred preferentially in *meta*-position than in *para*-position.

According to the dissociation energy of C-Cl bond in different positions, the possible dechlorination pathways of PCB-99 were predicted as shown in Fig. 6(a). First, the chlorine was removed at the *ortho*-position, then the chlorine was removed at the *meta*-position, and finally removed at the *para*-position to generate biphenyl. As could be seen that the C-Cl bond dissociation energy at 2′ position of PCB-99 was the lowest (86.9817 kcal mol^{-1}), which was the most easily broken. As a result, PCB-74 was produced after removing the chlorine at the 2′ position of PCB-99, and subsequently decomposed into PCB-37 after removing the chlorine at the 2 position (85.7241 kcal mol^{-1}). Afterward, as the chlorine at the 3 position (87.7497 kcal mol^{-1}) and 4 or 4′ position (87.7497 kcal mol^{-1}) was removed successively, PCB-37 was first transformed into PCB-15, then formed PCB-3, and finally degraded into biphenyl.

3.4.2. Length changes of neutral molecules and anionic C-Cl bonds

The structures of neutral molecules and anions of PCBs were listed in Table S5. No imaginary frequency was showed in all the optimized structures, indicating that they were the minimum energy structures. The results showed that the neutral molecules of PCBs were significantly different from anions, and the C-Cl bond of anions were elongated and even broken. The length changes of C-Cl bond between neutral molecules and anions were calculated, as shown in Table S6. The elongated C-Cl bond of the PCB anion was located on the benzene ring side of the chlorine substituted group, and the order of the elongated C-Cl bond was generally as followed: *meta*- > *ortho*- > *para*-position. The longer the C-Cl bond length was, the easier it was to fracture. Therefore, the possible dechlorination products and pathways of PCB-99 according to the changes of the C-Cl bond length were predicted, as shown in Fig. 6(b). The length of C-Cl bond at the 5 position was 1.748 Å in the neutral state and 2.999 Å in the anionic state, which was more prone to be broken. Therefore, the chlorine at the 5 position of PCB-99 was removed to form PCB-47. After that, the C-Cl at the 2 or 2′ position of PCB-47 was broken to form PCB-28. As for PCB-28, the length of C-Cl bond at the 2 position was 1.763 Å in the neutral state and 4.617 Å in the anionic state, it was more fragile and prone to be broken, resulting in the generation of PCB-15. Finally, PCB-15 was dechlorinated at the *para*-position, and further degraded into PCB-3 and biphenyl.

3.4.3. The LUMO configuration

The energy of LUMO could characterize the electron acceptance characteristics of the compound. The lower the absolute value of the

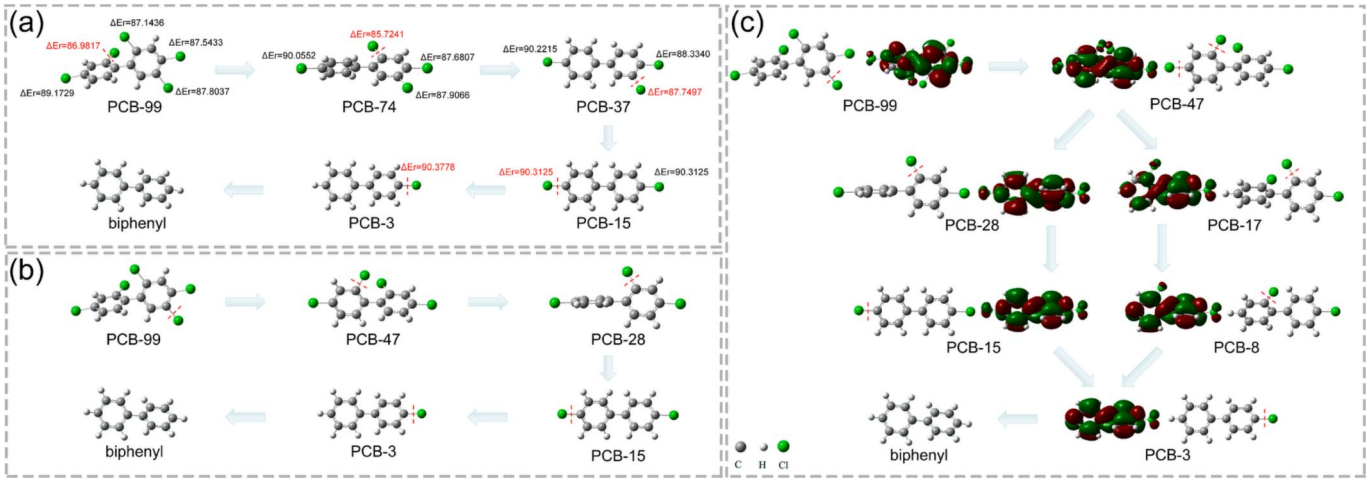

Fig. 6. Possible dechlorination pathways of PCB-99 based on (a) bond dissociation energy (kcal mol^{-1}); (b) the C-Cl bond length; (c) the LUMO of PCBs anions.

LUMO energy value, the easier PCBs was to accept electrons and be dechlorinated[65]. The LUMO configurations of PCB-99 and other 24 dechlorination products were optimized, as shown in Fig. S2. It could be seen that more LUMO was distributed on the side of the benzene ring with more chlorine, thus there were more active sites and dechlorination was more likely to occur[66]. Chlorine substituents at different positions had different effects on the energy of LUMO. According to the energy of LUMO: PCB-1 (*ortho*-position) > PCB-3 (*para*-position) > PCB-2 (*meta*-position), it could be inferred that chlorine at the *meta*-position made the LUMO energy of PCBs lower. The same regularity could be applied to dichlorinated biphenyls (PCB-8 > PCB-15 > PCB-13), as well as trichlorodiphenyl (PCB-17 > PCB-28 > PCB-25).

Moreover, the neutral molecules of PCBs received electrons provided by Ni/Fe to form PCBs anions. Electrons entered LUMO and resulted in obvious C-Cl anti-bonding orbital characteristics of LUMO, facilitating the breakage of C-Cl bond. Therefore, the dechlorination pathway could be effectively predicted by the LUMO of the anion[8]. As could be seen in Fig. 6(c), the LUMO of PCB-99 anion had greater C-Cl anti-bonding characteristics at the 5 position than at other positions, which should be preferentially removed, resulting in the removal of chlorine from 5 position of PCB-99 and the generation of PCB-47. The LUMO distribution of PCB-47 anion was relatively uniform, and the chlorine substituents of both *ortho*- and *para*-positions were likely to break. However, as previously discussed, it could be concluded that C-Cl at *para*-position was relatively easier to remove than at *ortho*-position. Therefore, PCB-47 might be degraded into PCB-28 or PCB-17 (the latter might generate more). The LUMO of PCB-28 and PCB-17 anions had a larger C-Cl anti-bonding characteristics at the 2 position, thus they might be preferentially removed. As a result, PCB-28 and PCB-17 mainly degraded to PCB-15 and PCB-8, respectively. PCB-8 was prone to degrade into PCB-3 because the LUMO of PCB-8 anion had a large C-Cl anti-bonding characteristics at the 2 position, while the chlorine substituent at the 4 position of PCB-15 was also easy to break and resulted in the generation of PCB-3. Finally, PCB-3 was further dechlorinated to biphenyl.

3.5. Dechlorination pathway confirmed by GC–MS

The dechlorination of PCB-99 on Ni/Fe surface could be explained by the mechanism of electrophilic aromatic substitution. To be specific, PCB congeners accepted electrons from Ni/Fe to form aromatic anions with the loss of Cl^-, and then aromatic anions were hydrogenated[67]. In order to confirm the chemical dechlorination pathway of PCB-99 over Ni/Fe, GC–MS chromatograms at different reaction times (2, 6, 12, 48, and 120 h) at 25 °C were investigated. The amount of electron transfer of Ni/Fe was different under different temperatures, but the reaction sites where these electrons attack PCB-99 should be the same. So the optimal condition of 25 ℃ was selected for GC–MS analysis, which could help to judge the accuracy of different quantum calculations in predicting the dechlorination pathways of PCB-99. Fig. S3 showed the chromatographic diagram of PCBs mixed solution. The chromatographic peaks of PCBs were separated well and the composition of dechlorination products could be determined.

Fig. S4 presented the GC–MS chromatograms during the catalytic dechlorination of PCB-99 at different reaction times. PCB-99, PCB-37, PCB-15, and PCB-3 existed after 2 h of reaction. PCB-99, PCB-47, PCB-37, and PCB-15 were presented after 6 h of reaction. PCB-99, PCB-37, PCB-28, PCB-17, and PCB-15 existed after 12 h of reaction. PCB-99, PCB-37, PCB-15, and PCB-3 were shown after 48 h of reaction. PCB-99, PCB-15, PCB-8, and biphenyl existed after 120 h reaction. The reason for the failure to detect PCB-74 might be its transitory existence during the dechlorination process, but the detection of PCB-37 indicated the presence of PCB-74 indirectly. According to the semi-quantitative analysis, the characteristic peak area of PCB-47 and PCB-17 were relatively higher than that of other PCB congeners, indicating that the dechlorination of PCB-99 showed obvious selectivity. It could be inferred that the main dechlorination pathway was PCB-99 → PCB-47 → PCB-17 → PCB-8 → PCB-3 → biphenyl, which also implied that electrons tended to attack C-Cl bonds following the order *meta*- > *para*- > *ortho*-position. In summary, the possible dechlorination pathways of PCB-99 based on GC–MS were shown in Fig. 7. These results were in good agreement with the dechlorination pathways predicted by quantum chemistry calculation, especially LUMO calculation, showing that the reduction path mediated by electron transfer was more consistent with the process of PCB-99 dechlorination, compared to C-Cl bond dissociation energy or bond length.

4. Conclusions

In this study, the catalytic dechlorination of PCB-99 by Ni/Fe was investigated, focusing on the electron transfer process. We specifically demonstrated that the reduction efficiency of PCB-99 did not always increase with the temperature increased from 15 °C to 35 °C, but followed the order: 25 °C > 15 °C > 35 °C. These unexpected results were related to the electron transfer process, and might be explained through one and/or a combination of the following reasons: (i) At 35 °C, the surface of Ni/Fe was heavily oxidized and particles aggregation occurred, hindering the electron transfer; (ii) Ni/Fe under the reaction condition of 25 °C could be attributed to the enhanced electron transfer due to the thermodynamic evolution of Fe species to generate more Fe (II) and the abundance of oxygen vacancies. Reaction temperature is

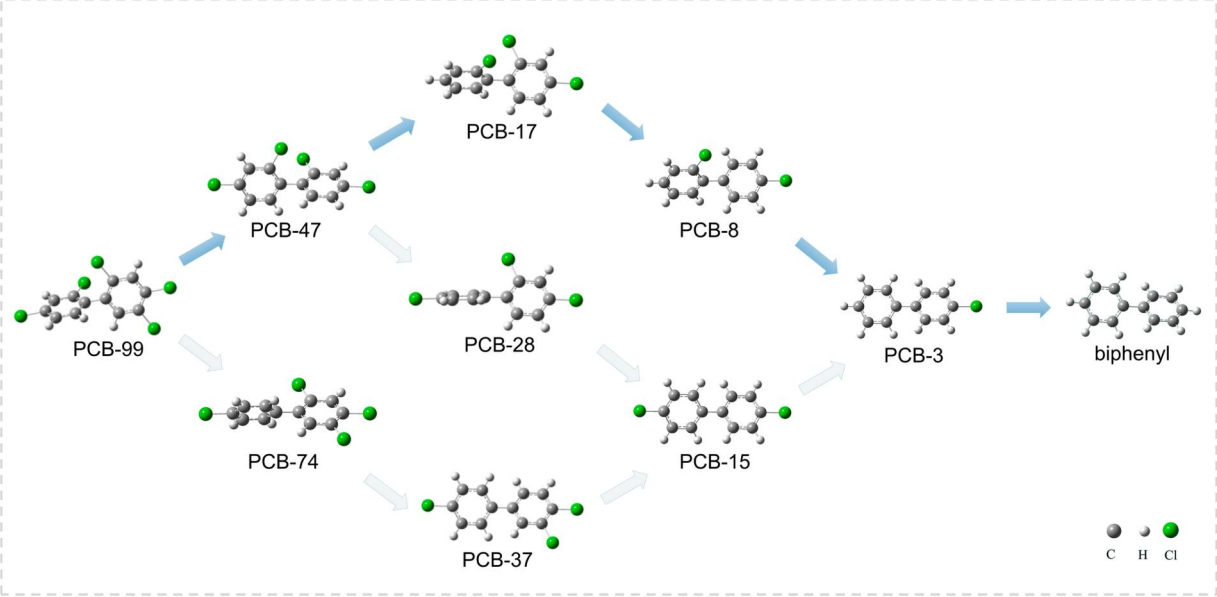

Fig. 7. Possible dechlorination pathways of PCB-99 based on GC–MS determination.

critical to investigate the kinetics of decontamination by Ni/Fe. In the actual application of ZVI-based materials to repair PCB pollution, it is necessary to control the appropriate temperature, which should be carefully considered from the aspects of remediation effect and cost. Additionally, the phenomenon of electron selectivity was elucidated by the quantum chemistry methods, which was consistent with the results of GC–MS, especially LUMO calculation. Electrons tended to attack C-Cl bonds in the order of *meta-* > *para-* > *ortho*-position. As a result, the dechlorination products of PCB-99 were PCB-74, PCB-47, PCB-37, PCB-28, PCB-17, PCB-15, PCB-8, PCB-3, and biphenyl. Particularly, the dechlorination of PCB-99 showed obvious selectivity and the main dechlorination pathway was PCB-99 → PCB-47 → PCB-17 → PCB-8 → PCB-3 → biphenyl. The dechlorination pathways and mechanism of PCB-99 can greatly improve our understanding of the electron transfer and dechlorination behaviors.

Declaration of Competing Interest

The authors declare that they have no known competing financial interests or personal relationships that could have appeared to influence the work reported in this paper.

Data availability

The authors do not have permission to share data.

Acknowledgements

The study was financially supported by the National Key R&D Program of China (No. 2019YFC1803900), the National Natural Science Foundation of China (No. 41907115), and Guangzhou Science and Technology Plan (No. 202102021025).

Appendix A. Supplementary data

Supplementary data to this article can be found online at https://doi.org/10.1016/j.cej.2023.144053.

References

[1] H. Tang, J. Wang, S. Zhang, H. Pang, X. Wang, Z. Chen, M. Li, G. Song, M. Qiu, S. Yu, Recent advances in nanoscale zero-valent iron-based materials: characteristics, environmental remediation and challenges, J. Clean. Prod. 319 (2021) 128641.
[2] Q. Li, Z. Chen, H. Wang, H. Yang, T. Wen, S. Wang, B. Hu, X. Wang, Removal of organic compounds by nanoscale zero-valent iron and its composites, Sci. Total Environ. 792 (2021) 148546.
[3] L.i. Liang, X. Li, Y. Guo, Z. Lin, X. Su, B.o. Liu, The removal of heavy metal cations by sulfidated nanoscale zero-valent iron (S-nZVI): The reaction mechanisms and the role of sulfur, J. Hazard. Mater. 404 (2021) 124057.
[4] H. Dong, G. Zeng, C. Zhang, J. Liang, K. Ahmad, P. Xu, X. He, M. Lai, Interaction between Cu^{2+} and different types of surface-modified nanoscale zero-valent iron during their transport in porous media, J. Environ. Sci. 32 (2015) 180–188.
[5] J. Shi, C. Long, A. Li, Selective reduction of nitrate into nitrogen using Fe-Pd bimetallic nanoparticle supported on chelating resin at near-neutral pH, Chem. Eng. J. 286 (2016) 408–415.
[6] H. Shen, D. Zhong, Y. Xu, H. Chang, H. Wang, C. Xu, J. Mou, N. Zhong, Polyacrylate stabilized ZVI/Cu bimetallic nanoparticles for removal of hexavalent chromium from wastewater, Environ. Sci. Pollut. Res. 30 (3) (2023) 5847–5860.
[7] F. Tian, J. Tang, J. Zeng, Z. Luo, L. Zhang, F. Tang, Z. Han, X. Yang, Degradation of atrazine by Ni-doped sulfidated microscale zero-valent iron: Mechanistic insights for enhanced reactivity and selectivity, Chem. Eng. J. 435 (2022) 135120.
[8] R. Wang, T. Tang, K. Huang, M. Zou, X. Tao, H. Yin, Z. Lin, Z. Dang, G. Lu, Debromination of polybrominated biphenyls (PBBs) by zero valent metals and iron-based bimetallic particles: Mechanisms, pathways and predicting descriptor, Chem. Eng. J. 351 (2018) 773–781.
[9] Q. Zhang, Y. Guo, M. Huang, H. Li, C. Gu, Degradation of selected polychlorinated biphenyls by montmorillonite clay-templated Fe^0/Ni^0 bimetallic system, Chem. Eng. J. 276 (2015) 122–129.
[10] M. Zhuang, W. Shi, H. Wang, L. Cui, G. Quan, J. Yan, Carbothermal Synthesis of Ni/Fe Bimetallic Nanoparticles Embedded into Graphitized Carbon for Efficient Removal of Chlorophenol, Nanomaterials 11 (6) (2021) 1417.
[11] J. Xu, L. Tan, S.A. Baig, D. Wu, X. Lv, X. Xu, Dechlorination of 2,4-dichlorophenol by nanoscale magnetic Pd/Fe particles: Effects of pH, temperature, common dissolved ions and humic acid, Chem. Eng. J. 231 (2013) 26–35.
[12] Z. He, K. Lin, J. Sun, L. Wen, C. Gao, J. Chen, S. Song, Y. Qian, W. Liu, Kinetics of electrochemical dechlorination of 2-chlorobiphenyl on a palladium-modified nickel foam cathode in a basic medium: From batch to continuous reactor operation, Electrochim. Acta 109 (2013) 502–511.
[13] Q. Sun, H. Zhou, M. Cao, et al., Degradation of 2,4-Dichlorophenol in Aqueous Solution by ZVI/EDDS /Air System, Chin. J. Environ. Sci. 33 (11) (2012) 3833–3839.
[14] B.o. Fan, X. Li, F. Zhu, J. Wang, Z. Gong, S. Shao, X. Wang, C. Zhu, D. Zhou, S. Gao, Anti-passivation ability of sulfidated microscale zero valent iron and its application for 1,1,2,2-tetrachloroethane degradation, J. Hazard. Mater. 443 (2023) 130194.
[15] L. Passatore, S. Rossetti, A.A. Juwarkar, A. Massacci, Phytoremediation and bioremediation of polychlorinated biphenyls (PCBs): state of knowledge and research perspectives, J. Hazard. Mater. 278 (2014) 189–202.
[16] B.-Z. Wu, H.-Y. Chen, S.J. Wang, C.M. Wai, W. Liao, KongHwa Chiu, Reductive dechlorination for remediation of polychlorinated biphenyls, Chemosphere 88 (7) (2012) 757–768.

[17] Z. Xiao, W. Jiang, D. Chen, Y. Xu, Bioremediation of typical chlorinated hydrocarbons by microbial reductive dechlorination and its key players: a review, Ecotoxicol. Environ. Saf. 202 (2020) 110925.

[18] K. Nomiyama, T. Tanizaki, H. Ishibashi, K. Arizono, R. Shinohara, Production Mechanism of Hydroxylated PCBs by Oxidative Degradation of Selected PCBs Using TiO_2 in Water and Estrogenic Activity of Their Intermediates, Environ. Sci. Tech. 39 (22) (2005) 8762–8769.

[19] H. Iwata, S. Tanabe, N. Sakai, R. Tatsukawa, Distribution of persistent organochlorines in the oceanic air and surface seawater and the role of ocean on their global transport and fate, Environ. Sci. Tech. 27 (6) (1993) 1080–1098.

[20] M. Ravanipour, I. Nabipour, M. Yunesian, N. Rastkari, A.H. Mahvi, Exposure sources of polychlorinated biphenyls (PCBs) and health risk assessment: a systematic review in Iran, Environ. Sci. Pollut. Res. 29 (37) (2022) 55437–55456.

[21] A. Cabrerizo, D.C.G. Muir, A.O. De Silva, X. Wang, S.F. Lamoureux, M.J. Lafrenière, Legacy and Emerging Persistent Organic Pollutants (POPs) in Terrestrial Compartments in the High Arctic: Sorption and Secondary Sources, Environ. Sci. Tech. 52 (24) (2018) 14187–14197.

[22] C.E. Shanahan, S.N. Spak, A. Martinez, K.C. Hornbuckle, Inventory of PCBs in Chicago and Opportunities for Reduction in Airborne Emissions and Human Exposure, Environ. Sci. Tech. 49 (23) (2015) 13878–13888.

[23] B.M. Sharma, L. Nizzetto, G.K. Bharat, S. Tayal, L. Melymuk, O. Sáňka, P. Přibylová, O. Audy, T. Larssen, Melting Himalayan glaciers contaminated by legacy atmospheric depositions are important sources of PCBs and high-molecular-weight PAHs for the Ganges floodplain during dry periods, Environ. Pollut. 206 (2015) 588–596.

[24] Q. Lu, Y. Liang, W. Fang, K.-L. Guan, C. Huang, X. Qi, Z. Liang, Y. Zeng, X. Luo, Z. He, B. Mai, S. Wang, Spatial Distribution, Bioconversion and Ecological Risk of PCBs and PBDEs in the Surface Sediment of Contaminated Urban Rivers: A Nationwide Study in China, Environ. Sci. Tech. 55 (14) (2021) 9579–9590.

[25] C.-a. Li, S.-S. Li, Y. Zhang, Y. Huang, L. Tao, Residues of polychlorinated biphenyls (PCBs) in a wild predatory fish from an e-waste site in South China between 2009 and 2016, Environ. Sci. Pollut. Res. 30 (3) (2023) 7303–7311.

[26] W. Han, J. Feng, Z. Gu, M. Wu, G. Sheng, J. Fu, Polychlorinated biphenyls in the atmosphere of Taizhou, a major e-waste dismantling area in China, J. Environ. Sci. (China) 22 (4) (2010) 589–597.

[27] G. Xu, S. Zhao, J. Liu, J. He, Bioremediation of organohalide pollutants: progress, microbial ecology, and emerging computational tools, Curr. Opin. Environ. Sci. Health. 32 (2023) 100452.

[28] G. Xu, X. Zhao, S. Zhao, J. He, Acceleration of polychlorinated biphenyls remediation in soil via sewage sludge amendment, J. Hazard. Mater. 420 (2021) 126630.

[29] R.B. Payne, U. Ghosh, H.D. May, C.W. Marshall, K.R. Sowers, A Pilot-Scale Field Study. In Situ Treatment of PCB-Impacted Sediments with Bioamended Activated Carbon, Environ. Sci. Tech. 53 (5) (2019) 2626–2634.

[30] A. Ševců, Y.S. El-Temsah, J. Filip, E.J. Joner, K. Bobčíková, M. Černík, Zero-valent iron particles for PCB degradation and an evaluation of their effects on bacteria, plants, and soil organisms, Environ. Sci. Pollut. Res. Int. 24 (26) (2017) 21191–21202.

[31] Y. Wu, Z. Wu, X. Huang, M.-O. Simonnot, T. Zhang, R. Qiu, Synergistical enhancement by Ni^{2+} and Tween-80 of nanoscale zerovalent iron dechlorination of 2,2',5,5'-tetrachlorinated biphenyl in aqueous solution, Environ. Sci. Pollut. Res. 22 (1) (2015) 555–564.

[32] Y. Wu, Y.u. Wang, X. Huang, M.-O. Simonnot, W. Wu, X. Cai, S. Chen, S. Wang, R. Qiu, W. Zhang, Surfactant-facilitated dechlorination of 2,2',5,5'-tetrachlorinated biphenyl using zero-valent iron in soil/sediment solution: Integrated effects of plausible factors, Chemosphere 212 (2018) 845–852.

[33] M. Bursch, J.-M. Mewes, A. Hansen, S. Grimme, Best-Practice DFT Protocols for Basic Molecular Computational Chemistry**, Angew. Chem. Int. Ed. 61 (42) (2022).

[34] G. Bo, L.i. Bo-Yu, Y. Shou-Liang, L.i. Yue-Hua, L.i. Guang-Yue, A time-dependent density functional theory study of a fluorescent probe to detect hydroxyl radicals: Inhibiting the twisted intramolecular charge-transfer process, Spectrochim. Acta A Mol. Biomol. Spectrosc. 260 (2021) 119928.

[35] S.e. Wang, C.e. Hao, Z. Gao, J. Chen, J. Qiu, Time-dependent density functional theory study on electronic excited states of the hydrogen-bonded solute-solvent phenol-(H_2O)n (n=3-5) clusters, J. Lumin. 131 (11) (2011) 2279–2285.

[36] Z. Zhang, S. Hu, S.A. Baig, J. Tang, X. Xu, Catalytic dechlorination of Aroclor 1242 by Ni/Fe bimetallic nanoparticles, J. Colloid Interface Sci. 385 (1) (2012) 160–165.

[37] W. Yan, A.A. Herzing, X.-Q. Li, C.J. Kiely, W.-X. Zhang, Structural Evolution of Pd-Doped Nanoscale Zero-Valent Iron (nZVI) in Aqueous Media and Implications for Particle Aging and Reactivity, Environ. Sci. Tech. 44 (11) (2010) 4288–4294.

[38] R. Wang, T. Tang, G. Lu, Z. Zheng, K. Huang, H. Li, X. Tao, H. Yin, Z. Shi, Z. Lin, F. Wu, Z. Dang, Mechanisms and pathways of debromination of polybrominated diphenyl ethers (PBDEs) in various nano-zerovalent iron-based bimetallic systems, Sci. Total Environ. 661 (2019) 18–26.

[39] D. Dutta, D.K. Dutta, Selective and efficient hydrogenation of halonitrobenzene catalyzed by clay supported Ni^0 -nanoparticles, Appl. Catal. A 487 (2014) 158–164.

[40] X. Weng, Q. Sun, S. Lin, Z. Chen, M. Megharaj, R. Naidu, Enhancement of catalytic degradation of amoxicillin in aqueous solution using clay supported bimetallic Fe/Ni nanoparticles, Chemosphere 103 (2014) 80–85.

[41] N. Gong, K. Shao, W. Feng, Z. Lin, C. Liang, Y. Sun, Biotoxicity of nickel oxide nanoparticles and bio-remediation by microalgae Chlorella vulgaris, Chemosphere 83 (4) (2011) 510–516.

[42] Y.-P. Sun, X.-Q. Li, J. Cao, W.-X. Zhang, H.P. Wang, Characterization of zero-valent iron nanoparticles, Adv. Colloid Interface Sci. 120 (1-3) (2006) 47–56.

[43] T. Yamashita, P. Hayes, Analysis of XPS spectra of Fe^{2+} and Fe^{3+} ions in oxide materials, Appl. Surf. Sci. 254 (8) (2008) 2441–2449.

[44] T. Liu, X. Li, T.D. Waite, Depassivation of Aged Fe^0 by Divalent Cations: correlation between Contaminant Degradation and Surface Complexation Constants, Environ. Sci. Tech. 48 (24) (2014) 14564–14571.

[45] X. Zhang, S. Lin, Z. Chen, M. Megharaj, R. Naidu, Kaolinite-supported nanoscale zero-valent iron for removal of Pb^{2+} from aqueous solution: Reactivity, characterization and mechanism, Water Res. 45 (11) (2011) 3481–3488.

[46] X. Weng, P. Sun, Y.u. Long, Q. Meng, Z. Wu, Catalytic Oxidation of Chlorobenzene over $Mn_xCe_{1-x}O_2$/HZSM-5 Catalysts: A Study with Practical Implications, Environ. Sci. Tech. 51 (14) (2017) 8057–8066.

[47] S. Yang, Z. Huang, P. Wu, Y. Li, X. Dong, C. Li, N. Zhu, X. Duan, D.D. Dionysiou, Rapid removal of tetrabromobisphenol A by α-Fe_2O_{3-x}@Graphene@Montmorillonite catalyst with oxygen vacancies through peroxymonosulfate activation: Role of halogen and α-hydroxyalkyl radicals, Appl Catal B 260 (2020) 118129.

[48] Y. Fang, S.R. Al-Abed, Dechlorination kinetics of monochlorobiphenyls by Fe/Pd: Effects of solvent, temperature, and PCB concentration, Appl Catal B 78 (3–4) (2008) 371–380.

[49] W.Y.D.C. Lü Guifang, Study on the mass transfer regulation in micro-scale Ni-Fe/PCBs system by humic acid and tween-80, Ecology and Environmental Sciences. 31 (7) (2022) 1456–1464.

[50] E.J. Reardon, Zerovalent irons: styles of corrosion and inorganic control on hydrogen pressure buildup, Environ. Sci. Tech. 39 (18) (2005) 7311–7317.

[51] R. Ferrando, J. Jellinek, R.L. Johnston, Nanoalloys: From Theory to Applications of Alloy Clusters and Nanoparticles, Chem. Rev. 108 (3) (2008) 845–910.

[52] O. Eljamal, R. Mokete, N. Matsunaga, Y. Sugihara, Chemical pathways of Nanoscale Zero-Valent Iron (NZVI) during its transformation in aqueous solutions, J. Environ. Chem. Eng. 6 (5) (2018) 6207–6220.

[53] K.B. Gregory, P. Larese-Casanova, G.F. Parkin, M.M. Scherer, Abiotic Transformation of Hexahydro-1,3,5-trinitro-1,3,5-triazine by FeII Bound to Magnetite, Environ. Sci. Tech. 38 (5) (2004) 1408–1414.

[54] S. Bae, K. Hanna, Reactivity of Nanoscale Zero-Valent Iron in Unbuffered Systems: Effect of pH and Fe(II) Dissolution, Environ. Sci. Tech. 49 (17) (2015) 10536–10543.

[55] J. Huang, A. Jones, T.D. Waite, Y. Chen, X. Huang, K.M. Rosso, A. Kappler, M. Mansor, P.G. Tratnyek, H. Zhang, Fe(II) Redox Chemistry in the Environment, Chem. Rev. 121 (13) (2021) 8161–8233.

[56] S. Wang, B. Gao, Y. Li, A.E. Creamer, F. He, Adsorptive removal of arsenate from aqueous solutions by biochar supported zero-valent iron nanocomposite: Batch and continuous flow tests, J. Hazard. Mater. 322 (2017) 172–181.

[57] A. Liu, J. Liu, J. Han, W.-X. Zhang, Evolution of nanoscale zero-valent iron (nZVI) in water: Microscopic and spectroscopic evidence on the formation of nano- and micro-structured iron oxides, J. Hazard. Mater. 322 (2017) 129–135.

[58] S. Bae, R.N. Collins, T.D. Waite, K. Hanna, Advances in Surface Passivation of Nanoscale Zerovalent Iron: A Critical Review, Environ. Sci. Tech. 52 (21) (2018) 12010–12025.

[59] M. Pan, S.-Y. Tang-Hu, C. Li, J. Hong, S. Liu, B. Pan, Oxygen vacancy-mediated peroxydisulfate activation and singlet oxygen generation toward 2,4-dichlorophenol degradation on specific CuO_{1-x} nanosheets, J. Hazard. Mater. 441 (2023) 129944.

[60] M. Singh, D. Jampaiah, A.E. Kandjani, Y.M. Sabri, E. Della Gaspera, P. Reineck, M. Judd, J. Langley, N. Cox, J. van Embden, E.L.H. Mayes, B.C. Gibson, S. K. Bhargava, R. Ramanathan, V. Bansal, Oxygen-deficient photostable Cu(2)O for enhanced visible light photocatalytic activity, Nanoscale 10 (13) (2018) 6039–6050.

[61] R. Wang, T. Tang, G. Lu, K. Huang, M. Chen, X. Tao, H. Yin, Z. Dang, Formation and degradation of polybrominated dibenzofurans (PBDFs) in the UV photolysis of polybrominated diphenyl ethers (PBDEs) in various solutions, Chem. Eng. J. 337 (2018) 333–341.

[62] F.M. Zullo, M. Liu, S. Zou, C.L. Yestrebsky, Mechanistic and computational studies of PCB 151 dechlorination by zero valent magnesium for field remediation optimization, J. Hazard. Mater. 337 (2017) 55–61.

[63] C. Li, J. Liu, N. Wu, X. Pan, J. Feng, G. Al-Basher, A.A. Allam, R. Qu, Z. Wang, Photochemical formation of hydroxylated polychlorinated biphenyls (OH-PCBs) from decachlorobiphenyl (PCB-209) on solids/air interface, J. Hazard. Mater. 378 (2019) 120758.

[64] S.e. Wang, C.e. Hao, Z. Gao, J. Chen, J. Qiu, Theoretical investigation on photodechlorination mechanism of polychlorinated biphenyls, Chemosphere 95 (2014) 200–205.

[65] H.K. Yak, Q. Lang, C.M. Wai, Relative Resistance of Positional Isomers of Polychlorinated Biphenyls toward Reductive Dechlorination by Zerovalent Iron in Subcritical Water, Environ. Sci. Tech. 34 (13) (2000) 2792–2798.

[66] Y. Zhuang, S. Ahn, R.G. Luthy, Debromination of Polybrominated Diphenyl Ethers by Nanoscale Zerovalent Iron: Pathways, Kinetics, and Reactivity, Environ. Sci. Tech. 44 (21) (2010) 8236–8242.

[67] Z. Yun, F. Fan, Z. Wu, M. Yin, L. Zhao, Z. Huang, H. Hou, Insight into degradation mechanism of PCBs from thermal desorption off-gas over iron-based catalysts, Chemosphere 286 (2022) 131925.